Direct Patterning of Gold Nanoparticles Using Dip-Pen Nanolithography

Wechung Maria Wang,[†] Randall M. Stoltenberg,[‡] Shuhong Liu,[§] and Zhenan Bao[†,*]

[†]Department of Chemical Engineering, [‡]Department of Chemistry, and [§]Department of Materials Science and Engineering, Stanford University, Stanford, California 94305

ABSTRACT Various methods for the patterned assembly of metal nanoparticles have been developed in order to harness their unique electrical and optical properties for device applications. This paper discusses a method for direct writing of Au nanoparticles at nanoscale resolution using dip-pen nanolithography. First, a procedure was developed for increasing the loading of Au nanoparticles onto AFM tips to prolong patterning life. AFM tips were subsequently imaged by scanning electron microscopy to determine ink coverage and to gain insight into the deposition process. Next, surface interactions, relative humidity, and writing speed were controlled to determine an optimal range of conditions for deposition. Various ink—substrate combinations were studied to elucidate the dependence of deposition on interactions between Au nanoparticles and the substrate surface; inks consisted of positively and negatively charged particles, and substrates were SiO_2 surfaces modified as hydrophilic or hydrophobic and interacted electrostatically or covalently with Au nanoparticles. Results indicate that a highly hydrophilic surface is required for Au nanoparticle deposition, unless covalent binding can occur between the Au and substrate surface. The optimal range of relative humidity for patterning was found to be 40—60%, and Au nanoparticle deposition was not sensitive to writing speeds ranging from 0.01 to 2 μm/s.

KEYWORDS: gold nanoparticles · patterning · scanning probe lithography · dip-pen nanolithography · silicon · nanofabrication

The patterned assembly of Au nanostructures has garnered much interest due to their unique electrical and optical properties,[1] which have led to several applications in electronics,[2−4] chemical[5] and biological[6] sensing, catalysis,[7] and optics.[8] To achieve precise ordering of these materials for devices, various patterning techniques such as electron-beam lithography and microcontact printing have been developed.[9] More recently, dip-pen nanolithography (DPN) has emerged as a scanning probe-based technique that combines the nanoscale resolution of electron-beam lithography with the direct writing of microcontact printing.[10] The versatility of DPN is evidenced by its wide range of substrates and inks such as alkanethiols,[11] silanes,[12,13] polyelectrolytes,[14,15] conducting polymers,[16−18] and biological molecules.[19−21]

In particular, DPN of 16-mercaptohexadecanoic acid has been used to generate a resist layer on Au films for patterning Au nanostructures on silicon.[22] However, this subtractive approach requires extra steps in coating the substrate surface with a thin film of Au and etching exposed Au. Additive methods, on the other hand, rely on the self-assembly of Au nanoparticles (NPs) on organic templates patterned by electrochemical atomic force microscopy (AFM).[23−25] Both of these indirect techniques involve more steps in lithography and surface modification than DPN of Au NPs.

Although DPN has been used for the direct write of Au NPs,[26−28] results in the literature conflict or are incomplete regarding the importance of various factors such as contact force and substrate effects. For instance, Thomas *et al.* reported that pattern dimensions were independent of the applied contact force, whereas Ben Ali *et al.* observed strong contact force dependence. Furthermore, Garno *et al.* used a covalent linkage between the Au NPs and the substrate surface to limit lateral diffusion of patterns; however, the need for such specific interactions has not been proven. Moreover, the extent of patterning was limited in all studies due to low throughput presumably caused by depletion of ink.

For continuous feeding of ink, a microfluidic nanofountain probe was developed and used to pattern arrays of Au NPs—resulting in dots as small as 200 nm in diameter[29] and lines as thin as 100 nm.[30] However, the resolution of these printed features was ultimately limited by the aperture of the nanofountain probe, which was fabricated *via* a multistep micromachining process. Other attempts at using a scanning probe tip for patterning Au nanostructures have involved application of electric

*Address correspondence to zbao@stanford.edu.

Received for review August 28, 2008 and accepted September 26, 2008.

Published online October 9, 2008.
10.1021/nn8005416 CCC: $40.75

fields,[31−33] surface reduction of Au salt,[34] and biocatalysis.[35]

We report a facile method using commercially available AFM tips for high-resolution, direct patterning of Au NPs on a variety of surfaces. Since ink transport is thought to occur *via* the water meniscus that forms between the AFM tip and the substrate,[36] the Au NPs used in this study were water soluble. Deposition of Au NPs occurs when their affinity for the substrate overcomes that for the tip and any cohesive forces within the ink itself. To promote transfer of ink to the substrate, the Au NPs were dispersed in either water or methanol, both low viscosity solvents, and then weakly physisorbed on the tip *via* an additive inking process. Furthermore, various ink−substrate combinations were studied to elucidate the dependence of deposition on interactions between Au NPs and the substrate surface; inks consisted of positively and negatively charged Au NPs, and substrates were similarly or oppositely charged, hydrophilic or hydrophobic, or capable of binding to Au *via* a thiol functionality.

This paper investigates five variables in the deposition process: ink loading, surface interactions, relative humidity (RH), writing speed, and ink−solvent system. First, a procedure was developed for increasing the loading of Au NPs onto AFM tips to prolong patterning life. Next, surface interactions, RH, and writing speed were varied to determine an optimal range of conditions for deposition. Other DPN inks such as alkanethiols have well-characterized behavior under a range of RH and writing speed;[37] however, to our knowledge, no such study has been reported for Au NPs. Finally, mixed solvent systems were formulated to impart more fluid-like properties to the Au NP ink.

RESULTS AND DISCUSSION

Ink Loading. The base inks used in this study consisted of aqueous solutions of negatively charged citrate-capped Au NPs (C-Au NPs, 5 nm nominal diameter), aqueous solutions of positively charged amine-capped Au NPs (Nanogold, 1.4 nm), and methanolic solutions of positively charged 4-(*N*,*N*-dimethylamino)pyridine-capped Au NPs (DMAP-Au NPs, average diameter 5 nm). The respective concentrations of C-Au NPs, Nanogold, and DMAP-Au NPs were approximately 5.1×10^{13}, 1.8×10^{16}, and 1.6×10^{15} particles/mL. Limited patterning occurred when the AFM tips were functionalized *via* the dip-coating method commonly used for DPN inks. The extent of patterning correlated with Au NP concentration; tips dip-coated with Nanogold and DMAP-Au NPs sometimes produced patterns, while C-Au NPs, which were of the lowest concentration, could not be patterned. Therefore, we developed an inking method for saturating Au NPs on AFM tips to achieve consistent patterning.

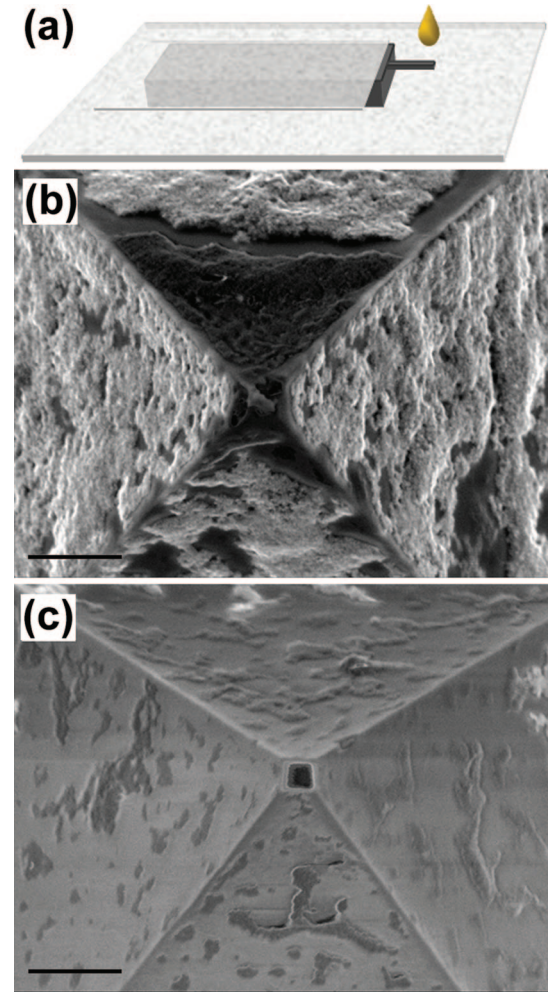

Figure 1. (a) Tip inking setup. The droplet of Au NPs is confined around the AFM tip by hydrophobic Parafilm surrounding the probe. SEM images were taken of an AFM tip loaded with Au NPs (b) and a depleted AFM tip after patterning (c). Scale bars: 500 nm.

The Au NPs were loaded onto a Si_3N_4 AFM tip *via* a micropipetter dispensing 5 μL droplets. To efficiently load the tip, the ink was confined to the cantilever by placing Parafilm under and on top of the probe (Figure 1a). The hydrophobic nature of Parafilm ensured that the droplets would stay on the cantilever at a high contact angle rather than spread to the rest of the probe. To concentrate the Au NPs on the tip, solvent evaporation was accelerated by heating the probe to 60−70 °C under a saturated water vapor environment. This inking procedure was repeated three to five times for sufficient loading of Au NPs, which was verified using scanning electron microscopy (SEM) in Figure 1b. A freshly coated tip was then used for continuous patterning until depletion of ink from the tip, again verified with SEM (Figure 1c). Typically, such inked tips deposited Au NP patterns spanning several microns.

Surface Interactions. The base substrate used in this study was silicon with a thermally grown oxide layer (300 nm). This SiO_2 surface is commonly used for device fabrication, well characterized, and easily function-

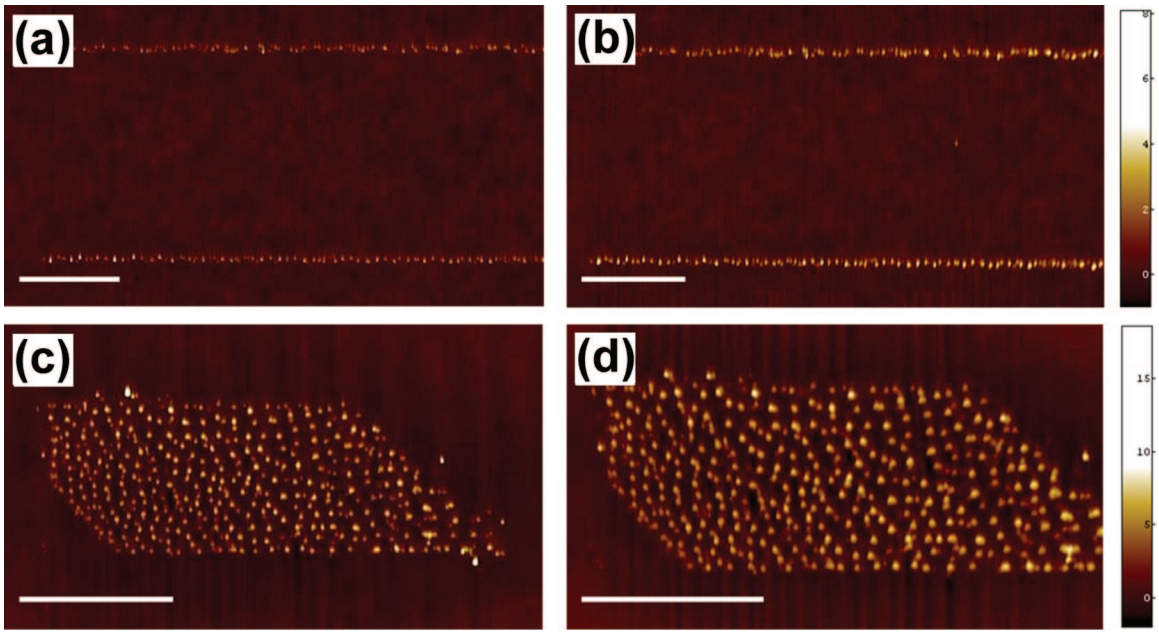

Figure 2. AFM topographic images of DMAP-Au NP patterns on UV-ozone cleaned SiO_2. Lines and boundary patterns before (a,c) and after (b,d) annealing at 165 °C for 30 min. Each pair of images (a,b) and (c,d) has the same height scale as shown on the right. Scale bars: 2 μm.

alized. To promote the formation of a water meniscus between the AFM tip and the substrate, the SiO_2 was rendered hydrophilic (static water contact angle ≈ 0°) by UV-ozone (UVO) treatment.

Since SiO_2 was negatively charged under the conditions of our deposition (above pH 3.5),[38] DPN of positively charged DMAP-Au NPs and Nanogold was attempted with the hypothesis that electrostatic attraction would aid Au NP printing. Both of these Au NPs were successfully patterned *via* DPN on UVO-treated SiO_2 at ambient temperatures and RH above 40%. Conditions such as RH and writing speed will be discussed in later sections.

Panels a and c of Figure 2 show AFM images of patterned DMAP-Au NPs. The heights of the particles in the line and boundary patterns are 2.5 ± 0.9 and 5.1 ± 1.9 nm, respectively. The thermal stability of these patterns was verified by annealing at 165 °C for 30 min (Figures 2b,d). The heights of the annealed particles were comparable to those before annealing: 3.3 ± 1.1 and 5.3 ± 1.3 nm for the line and boundary patterns, respectively.

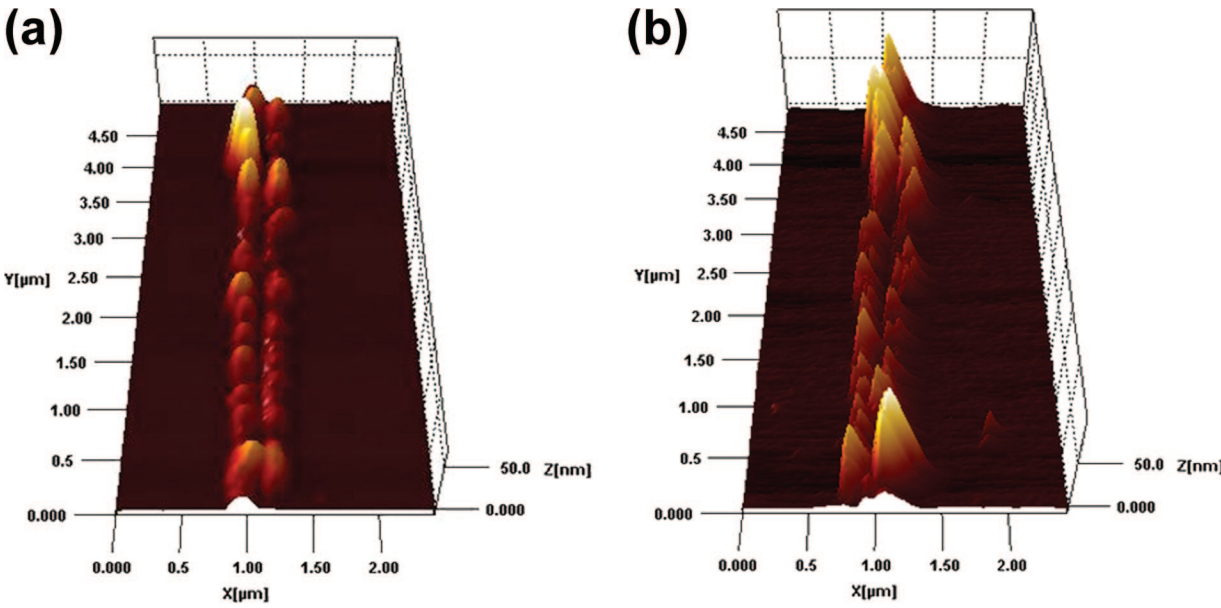

Figure 3. AFM topographic images rendered in 3D of Nanogold patterns on UV-ozone cleaned SiO_2 before (a) and after (b) gold development.

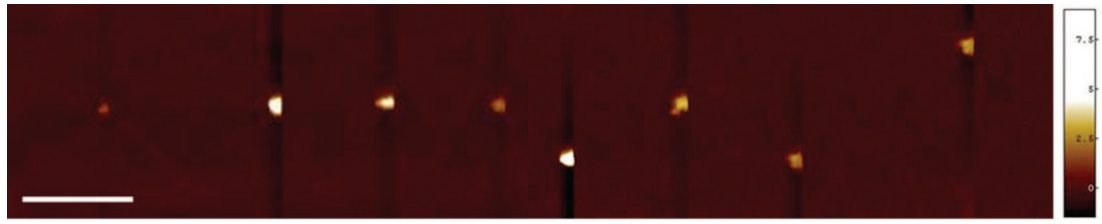

Figure 4. AFM topographic image of C-Au NP patterns on poly-L-lysine/SiO_2. The dot patterns were purposefully offset for ease of identification. Scale bar: 2 μm.

On the basis of analysis of DMAP-Au NPs by transmission electron microscopy (see Supporting Information, Figure S1), particle size ranges from 1 to 8 nm. Since the lines were patterned before the boundary pattern using the same inked tip, we can conclude that smaller particles deposit first, followed by larger particles and aggregates. This result has also been observed with C-Au NPs (see section titled Writing Speed) and is in accordance with the Stokes−Einstein equation, which predicts that smaller particles have a higher diffusivity.[39]

The high diffusivity of Nanogold resulted in patterning of aggregates (Figure 3a), as opposed to the single-particle deposition observed for DMAP-Au NPs. The valley in the middle of the patterned line in Figure 3a is due to Nanogold depositing from the sides of the AFM tip onto the substrate.[40] To verify that the deposited material was indeed composed of Au NPs, the pattern was exposed to an electroless gold development solution (GoldEnhance EM from Nanoprobes, Inc.) for 5 min. Subsequent AFM scans revealed that the Au NPs approximately doubled in height (Figure 3b).

DPN of negatively charged Au NPs on a positively charged substrate was also demonstrated by using C-Au NPs as the ink and SiO_2 treated with poly-L-lysine as the substrate. The resultant patterns of Au NP dots are shown in Figure 4. The goal of dot patterning is to deposit a single Au NP in a precise location. Line patterns of C-Au NPs on poly-L-lysine-treated SiO_2 are also shown in the section titled Writing Speed. To verify that the deposited material was indeed Au, chemical analysis was performed on patterned C-Au NPs *via* Auger electron spectroscopy (AES). Preliminary AES spectra indicated high carbon content, and no Au peak was observed. The carbon signal was likely from citrate ions that comprise the ink matrix to stabilize the Au colloid. Since Auger electrons have a mean escape path of a few nanometers at most, an adequate signal from Au was detected only after eliminating the organic layers *via* thermal annealing and UVO cleaning of the patterns. Figure 5a shows an SEM of the Au features and the corresponding AES spectrum, which contains the Au (MNN) transitions at 2018 and 2100 eV. The peak for the Au (NVV) transition is not shown because it is convoluted with the low energy peak for SiO_2.

The AES data indicate that the DPN-generated patterns were indeed composed of Au NPs; however, it seems that the organic matrix stabilizing the Au NPs was also deposited. In fact, treatment of patterned DMAP-Au NPs and C-Au NPs with gold development solution resulted in significantly less growth than that of patterned Nanogold, which is not suspended with organic stabilizers in solution and hence more of the Au surface is exposed for reaction. Furthermore, AES analysis of AFM tips freshly inked with C-Au NPs indicates the presence of an organic matrix. The Auger spectrum in Figure 5b contains peaks for C (265 eV), O (510 eV), and Na (994 eV), reflecting the composition of sodium citrate, as well as weaker peaks for Au.

Despite the significant amount of negatively charged citrate ions comprising the ink, C-Au NPs were also successfully patterned on UVO-treated SiO_2 (Figure

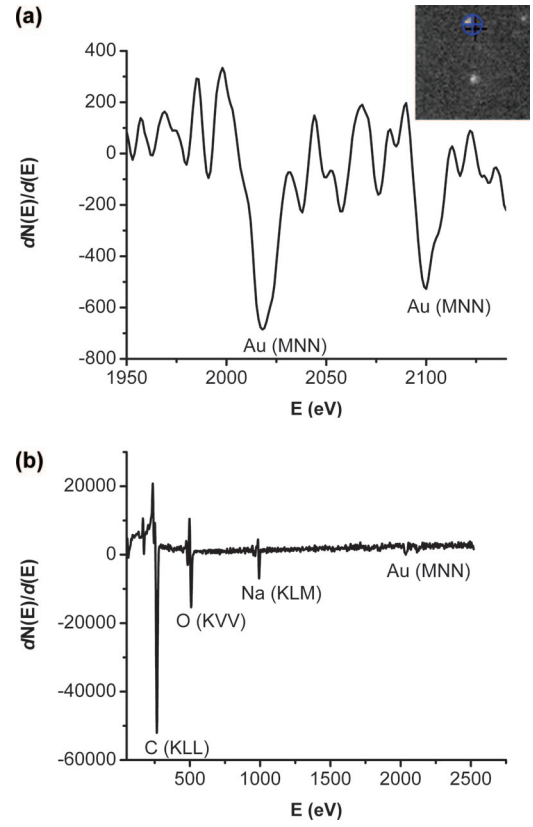

Figure 5. (a) Derivatized Auger spectrum of C-Au NPs deposited by DPN. The Au (MNN) transitions are labeled. Inset shows a 390 × 390 nm^2 SEM image of the C-Au NPs. Crosshair indicates point of analysis. (b) Derivatized Auger spectrum of an AFM tip inked with C-Au NPs. The C, O, and Na peaks are labeled and are indicative of a sodium citrate matrix surrounding the Au NPs.

6a), thereby demonstrating that negatively charged particles can be deposited *via* DPN on negatively charged substrates. As opposed to most DPN studies in which electrostatic attraction or covalent binding is required for patterning, the mechanism for Au NP patterning involves physisorption. Similar patterns were generated for both positively and negatively charged Au NPs on UVO-treated SiO_2. Therefore, these results suggest that electrostatic attraction between Au NPs and the substrate surface is not necessary for patterning.

Subsequent experiments were performed to determine whether a highly hydrophilic surface is a key requirement for Au NP patterning. Indeed, no deposition of Au NPs was observed on moderately hydrophilic to hydrophobic substrates in the absence of covalent interactions. SiO_2 functionalized with mercaptopropyltrimethoxy silane (MPTS-SiO_2, static water contact angle $\approx$ 45°) did not yield Au NP deposition unless the Au surface was available for covalent binding to the thiol groups. Only Nanogold particles were successfully patterned on MPTS-SiO_2; DMAP- and C-Au NPs did not deposit on this surface because the Au surfaces were covered in an organic matrix and thus not accessible for thiol binding.

The Nanogold line patterns on MPTS-SiO_2 (Figure 6b) are almost an order of magnitude lower in height than those on UVO-treated SiO_2 (Figure 3), suggesting different mechanisms for Nanogold deposition on these two surfaces. The driving force for Nanogold deposition on UVO-treated SiO_2 is the hydrophilic surface, whereas Nanogold deposits on MPTS-SiO_2 due to covalent binding. The less hydrophilic MPTS-SiO_2 surface may result in a smaller water meniscus forming at the AFM tip/substrate interface, thereby limiting the Au NP deposition.

In contrast to nanofountain probe studies,[29] C-Au NPs could not be deposited *via* DPN on SiO_2 functionalized with aminopropyltrimethoxy silane (static water contact angle $\approx$ 65°) despite the electrostatic attraction between C-Au NPs and the positively charged amino groups. The nanofountain probe patterned a liquid residue (consisting of sodium citrate) along with C-Au NPs; however, no such residue has been observed in attempted DPN of C-Au NPs on amino-terminated surfaces. Furthermore, DPN of Au NPs on SiO_2 functionalized with pentafluorophenyl propyl trichlorosilane (static water contact angle $\approx$ 84°) did not result in deposition, even at RH as high as 70%. These results indicate that a highly hydrophilic surface is required for DPN of Au NPs, unless covalent binding can occur between the Au NPs and the substrate surface. Electrostatic attraction is neither a necessary nor sufficient condition for DPN of Au NPs. These conclusions are consistent with reports on the importance of the water meniscus for ink transport in DPN.[16,36,40,41]

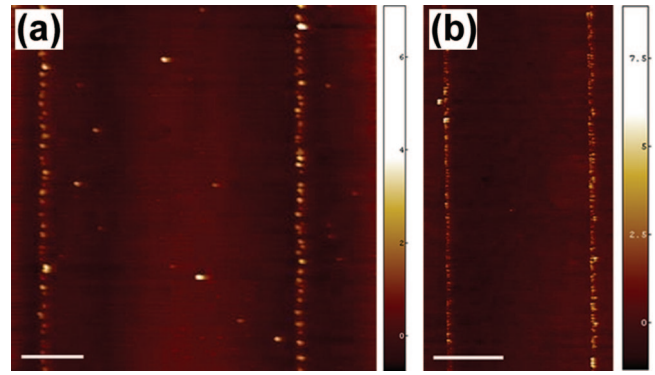

Figure 6. AFM topographic images of C-Au NP line patterns on UVO-treated SiO_2 (a) and Nanogold line patterns on mercaptopropyltrimethoxy silane-treated SiO_2 (b). Scale bars: 2 μm.

Relative Humidity. To further investigate the role of water in this system, multi-pen experiments under various relative humidity conditions were performed. Using an AFM probe with multiple tips (shown in Figure 7a) allowed for a high-throughput evaluation of RH effects while taking into account potential variations in the inking of each tip. In these nine experiments done in parallel, no Au NPs deposited at RH below 40%. All pens began patterning single-particle lines at RH 40%; a representative AFM image is shown in Figure 7b. As

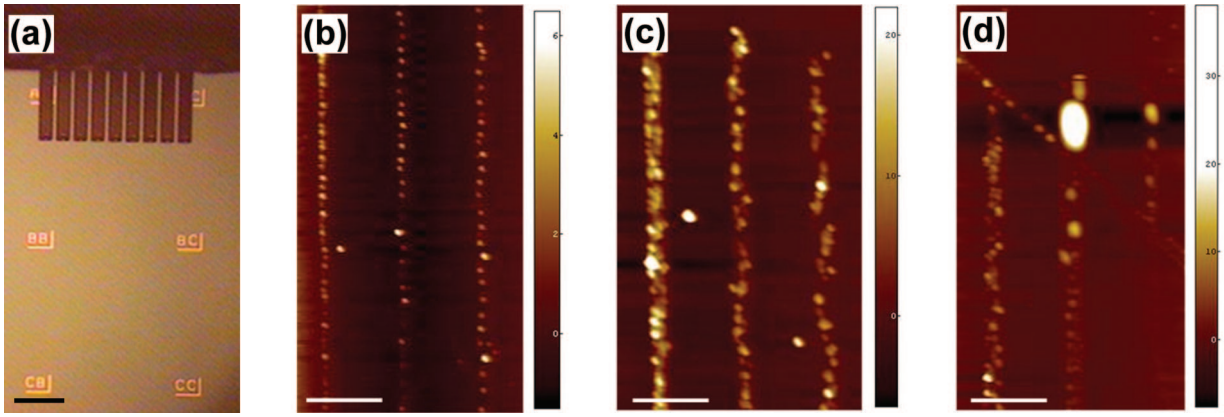

Figure 7. (a) Optical micrograph of multipen setup. All nine pens were used for patterning C-Au NPs at various relative humidities on UVO-treated SiO_2. Scale bar: 100 μm. (b–d) AFM topographic images of C-Au NPs patterned on UVO-treated SiO_2 at relative humidities of 40% (b), 60% (c), and 70% (d). Scale bars: 2 μm.

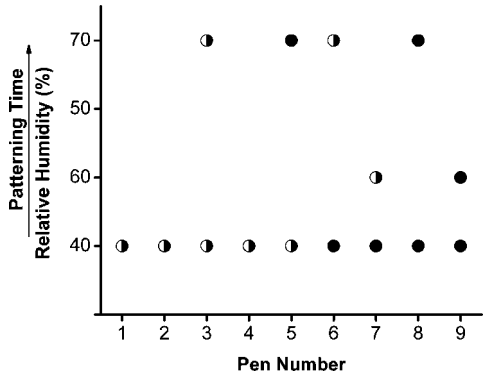

Figure 8. Plot of Au NP deposition for each of the nine pens on the DPN probe at various relative humidities as patterning time increases. The half-filled circles denote partial patterning, and the black circles denote complete patterning.

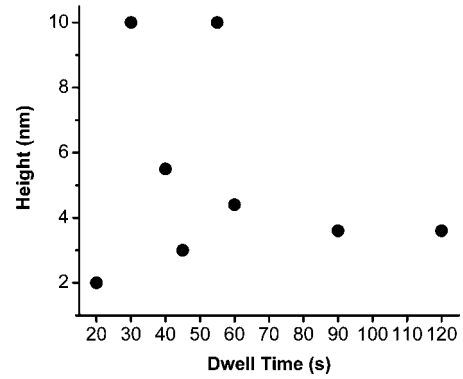

Figure 9. Plot of the measured heights of Au NPs in Figure 4 *versus* their respective tip dwell times. The data indicate that the amount of Au NPs deposited does not depend on tip dwell time for times ranging from 20 to 120 s.

RH increased to 60% and patterning progressed, the height and line width of patterns also increased as Au NP aggregates were deposited and tip blunting occurred due to prolonged contact with the surface (Figure 7c). At RH of 70%, co-deposition of the solvent matrix was observed (Figure 7d). A larger water meniscus at higher relative humidity[36,42] contributed to matrix deposition. Therefore, the optimal range for patterning Au NPs is RH of 40−60%.

Figure 8 illustrates the large tip-to-tip variation in patterning of Au NPs. The pens are numbered 1−9 from left to right in Figure 7a. At RH 40%, pens 1−5 produced only partial patterning of Au NPs, whereas pens 6−9 produced complete patterning. The right side of the pen array (pens 6−9) may have produced better patterning due to initial contact with the substrate, despite optical leveling of the entire array prior to patterning. When RH was ramped up to 60%, only pens 7 and 9 deposited Au NPs. When RH was decreased to 50%, none of the pens deposited Au NPs; therefore, as ink is depleted from the tip, the RH needs to be ramped up for continuous deposition. Patterning resumed for about half the pens when RH was increased to 70%. SEM analysis of all pens after patterning suggests that the discrepancy in deposition was due to variable contact between the pens and substrate surface. For instance, pens 3 and 5 were blunter than pens 1, 2, and 4 (Supporting Information, Figure S2).

Writing Speed. The start-and-stop deposition of partial patterns (Figure 7d) indicates that DPN of Au NPs is an inhomogeneous process. Further evidence for this inhomogeneity is the fact that deposition is independent of writing speed or tip dwell time. No correlation between tip dwell time and Au NP deposition could be found for times ranging from 20 to 120 s (Figure 9). Therefore, a diffusion coefficient could not be calculated for the transport of Au NPs from the tip to the substrate surface. Unlike inks such as small molecules and polymers, Au NPs do not spread laterally on substrates with increasing contact times. Single Au NPs were observed to deposit at dwell times of both 1 and 120 s. The Au NPs may stick on transfer and form a physical barrier against further deposition.

For line patterns, writing speeds ranging from 0.01 to 2 μm/s also did not have any correlation with Au NP deposition. As discussed in the previous section Surface Interactions, Au NPs exhibit a consistent diffusion profile with smaller particles depositing first followed by progressively larger particles as patterning proceeds. This phenomenon is illustrated in Figure 10 as writing speed is held constant at 1 μm/s. The discontinuities in Au NP deposition may be due to the time required for the particles to diffuse from the sides of the tip to the apex. A closer examination of the SEM image of an inked tip (Figure 1b) reveals islands of Au NPs that may contribute to the lag times in deposition. The variable particle sizes within each line in Figure 10 are also indicative of inhomogeneous deposition. Optimization of the Au NP ink is necessary to achieve more uniform

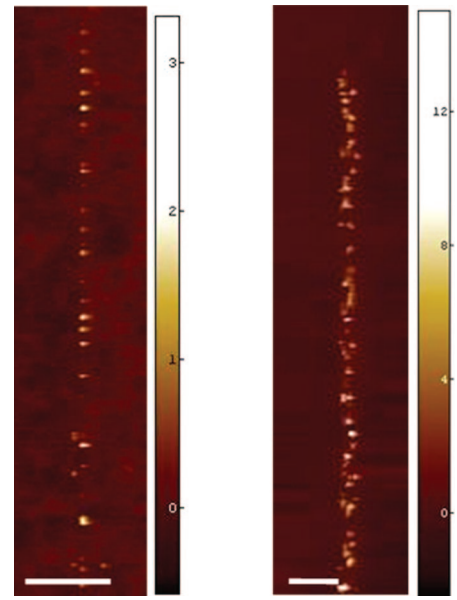

Figure 10. AFM topographic images of C-Au NPs patterned on poly-L-lysine-treated SiO_2. Lines were written at the same speed of 1 μm/s, and patterning progressed from left to right. Scale bars: 1 μm.

coating of the AFM tip and homogeneous Au NP deposition.

Ink−Solvent Systems. Preliminary experiments with different ink−solvent systems were conducted to investigate their effect on ink loading and subsequent deposition. Hexanol was added to DMAP-Au NPs in a 1:1 ratio to investigate its potential as a lubricating agent since it has a higher boiling point than methanol (151.4 °C *versus* 64.7 °C). The resultant DPN-generated patterns consisted only of the solvent matrix (Supporting Information, Figure S3). In another experiment, varying concentrations of ethylene glycol (boiling point: 197.3 °C) were added to C-Au NPs. At 10% incorporation of ethylene glycol, only the solvent matrix was deposited. No Au NP deposition was observed for 1% ethylene glycol incorporation either. Au NPs were only patterned when there was 0.1% or less ethylene glycol present in the ink. This small percentage of ethylene glycol did not significantly affect the patterning of Au NPs. Other ink−solvent combinations, however, could potentially result in more homogeneous patterning. In fact, studies in the literature have used surfactants for assisting DPN of biomolecules.[43]

CONCLUSIONS

We have developed a procedure for loading sufficient amounts of Au NPs onto AFM tips for patterning on various surfaces, which either need to be highly hydrophilic or covalently bind Au. The Au NPs have a diffusion profile consistent with the Stokes−Einstein equation and, unlike other DPN inks such as 16-mercaptohexadecanoic acid, Au NPs do not diffuse laterally on the substrate surface during deposition. The patterns were verified as Au NPs using chemical development of the Au and elemental analysis *via* AES. Patterning only occurs at RH $\geq$ 40%, with the optimal range being 40−60%, and is not sensitive to writing speeds ranging from 0.01 to 2 μm/s. Further developments in the formulation of Au NP inks and possibly surface modification of AFM tips are necessary to achieve more uniform coating of the tips and more homogeneous Au NP deposition.

METHODS

Au NPs. C-Au NPs were obtained from Sigma-Aldrich; Nanogold particles were obtained from Nanoprobes, Inc., and DMAP-Au NPs were synthesized according to a published procedure.[44] Briefly, 9 mg of $AuCl_3$ was dissolved by sonication in 3 mL of 100 mM didodecyldimethylammonium bromide (DDAB) in toluene. Next, 0.06 mL of tetrabutylammonium hydroxide (37% in methanol) was added, turning the solution from orange to yellow. Finally, 30 mg of tetrabutylammonium borohydride dissolved in 1.2 mL of DDAB solution was injected to the gold salt solution under stirring and N_2 purging. After 3 h, ligand exchange was performed by precipitating the Au NPs with a few drops of methanol/ethanol and centrifuging for 5 min at 14 000 rpm. The Au NPs were then resuspended in a methanolic solution of 0.1 M DMAP. Particle concentration was determined by UV−vis spectroscopy (assuming an extinction coefficient of 10^7 based on an average particle size of 5 nm[45]). Refer to Supporting Information, Figure S4 for the UV−vis spectrum.

Surface Preparation. Silicon wafers with 300 nm thermally grown oxide layers (Silicon Quest International) were diced into centimeter-sized pieces. Markers were scratched into the silicon using a diamond scribe to enable registration of the imaging tip with Au NP patterns. For relative humidity studies, a silicon substrate with lithographically patterned markers was obtained from Nanoink, Inc. All substrates were cleaned for at least 20 min in a UV-ozone cleaner (Model 42, Jelight Company Inc.) before further surface modification and patterning.

Surface treatment with poly-L-lysine (Ted Pella, Inc.) followed previously published protocol.[46] Briefly, SiO_2 pieces were exposed to a poly-L-lysine solution (1 ppm in water) for 3−5 min and then rinsed with deionized water. SiO_2 was functionalized with mercaptopropyltrimethoxy silane through immersion in a 2% v/v solution in ethanol overnight at room temperature. The substrates were then rinsed with and sonicated in ethanol and cured in an 80 °C oven for 30 min. Amino functionalization of SiO_2 occurred through vapor deposition of aminopropyltrimethoxy silane under vacuum overnight. Finally, hydrophobic SiO_2 was obtained by vapor deposition of pentafluorophenylpropyltrichlorosilane under vacuum and heating at 80 °C for 30 min. All silanes were obtained from Gelest, Inc.

Patterning and Imaging. Patterning (contact mode, setpoint 1.5 to 2 V) and imaging (AC mode) were performed on an NSCRIPTOR DPN system (Nanoink, Inc.) at ambient temperatures (26 ± 4 °C) and variable relative humidity set by the environmental chamber. Line, dot, and boundary patterns were created using InkCAD software, which allowed for the specification of writing speeds and dwell times. Au NPs were inked onto the diving-board cantilevers of types A and C Si_3N_4 probes (nominal spring constants 0.041 and 0.061 N/m, respectively) obtained from Nanoink, Inc. Au NP patterns were imaged using Si probes obtained from Nanoink, Inc. and Nanosensors, with nominal force constants of 42 N/m and nominal resonance frequencies of 320−330 kHz. AFM images were flattened using the Scanning Probe Image Processor (SPIP, Image Metrology A/S).

AFM tips were imaged on an FEI XL30 Sirion SEM operated at acceleration voltages ranging from 2 to 5 kV. AES data were taken on a PHI 700 Auger Nanoprobe (Physical Electronics, Inc.).

Acknowledgment. We thank C. Hitzman for his generous assistance with AES. This work was funded in part by a Center for Probing the Nanoscale, NSF Grant PHY-0425897. W.M.W. is supported by a Stanford Graduate Fellowship and an NSF Graduate Research Fellowship.

Supporting Information Available: TEM and UV−vis analysis of DMAP-Au NPs (Figures S1 and S4). SEM images of AFM tips in multi-pen probe after patterning (Figure S2). AFM of solvent matrix deposition after DPN with DMAP-Au NPs in methanol/hexanol (Figure S3). This material is available free of charge *via* the Internet at http://pubs.acs.org.

REFERENCES AND NOTES

1. Daniel, M. C.; Astruc, D. Gold Nanoparticles: Assembly, Supramolecular Chemistry, Quantum-Size-Related Properties, and Applications toward Biology, Catalysis, and Nanotechnology. *Chem. Rev.* **2004**, *104*, 293–346.
2. Liu, S. H.; Tok, J. B. H.; Bao, Z. Nanowire Lithography: Fabricating Controllable Electrode Gaps Using Au−Ag−Au Nanowires. *Nano Lett.* **2005**, *5*, 1071–1076.
3. Wu, Y. L.; Li, Y. N.; Ong, B. S.; Liu, P.; Gardner, S.; Chiang, B. High-Performance Organic Thin-Film Transistors with Solution-Printed Gold Contacts. *Adv. Mater.* **2005**, *17*, 184–187.
4. Ongaro, A.; Griffin, F.; Beecher, P.; Nagle, L.; Iacopino, D.; Quinn, A.; Redmond, G.; Fitzmaurice, D. DNA-Templated Assembly of Conducting Gold Nanowires between Gold

Electrodes on a Silicon Oxide Substrate. *Chem. Mater.* **2005**, *17*, 1959–1964.
5. Keebaugh, S.; Kalkan, A. K.; Nam, W. J.; Fonash, S. J. Gold Nanowires for the Detection of Elemental and Ionic Mercury. *Electrochem. Solid-State Lett.* **2006**, *9*, H88–H91.
6. Cao, Y. W. C.; Jin, R. C.; Mirkin, C. A. Nanoparticles with Raman Spectroscopic Fingerprints for DNA and RNA Detection. *Science* **2002**, *297*, 1536–1540.
7. Hughes, M. D.; Xu, Y.-J.; Jenkins, P.; McMorn, P.; Landon, P.; Enache, D. I.; Carley, A. F.; Attard, G. A.; Hutchings, G. J.; King, F.; et al. Tunable Gold Catalysts for Selective Hydrocarbon Oxidation under Mild Conditions. *Nature* **2005**, *437*, 1132–1135.
8. Maier, S. A.; Friedman, M. D.; Barclay, P. E.; Painter, O. Experimental Demonstration of Fiber-Accessible Metal Nanoparticle Plasmon Waveguides for Planar Energy Guiding and Sensing. *Appl. Phys. Lett.* **2005**, *86*, 071103-1–071103-3.
9. Xia, Y. N.; Rogers, J. A.; Paul, K. E.; Whitesides, G. M. Unconventional Methods for Fabricating and Patterning Nanostructures. *Chem. Rev.* **1999**, *99*, 1823–1848.
10. Salaita, K.; Wang, Y. H.; Mirkin, C. A. Applications of Dip-Pen Nanolithography. *Nat. Nanotechnol.* **2007**, *2*, 145–155.
11. Piner, R. D.; Zhu, J.; Xu, F.; Hong, S. H.; Mirkin, C. A. "Dip-Pen" Nanolithography. *Science* **1999**, *283*, 661–663.
12. Jung, H.; Kulkarni, R.; Collier, C. P. Dip-Pen Nanolithography of Reactive Alkoxysilanes on Glass. *J. Am. Chem. Soc.* **2003**, *125*, 12096–12097.
13. Kooi, S. E.; Baker, L. A.; Sheehan, P. E.; Whitman, L. J. Dip-Pen Nanolithography of Chemical Templates on Silicon Oxide. *Adv. Mater.* **2004**, *16*, 1013–1016.
14. Yu, M.; Nyamjav, D.; Ivanisevic, A. Fabrication of Positively and Negatively Charged Polyelectrolyte Structures by Dip-Pen Nanolithography. *J. Mater. Chem.* **2005**, *15*, 649–652.
15. Lee, S. W.; Sanedrin, R. G.; Oh, B. K.; Mirkin, C. A. Nanostructured Polyelectrolyte Multilayer Organic Thin Films Generated *via* Parallel Dip-Pen Nanolithography. *Adv. Mater.* **2005**, *17*, 2749–2753.
16. Lim, J. H.; Mirkin, C. A. Electrostatically Driven Dip-Pen Nanolithography of Conducting Polymers. *Adv. Mater.* **2002**, *14*, 1474–1477.
17. Maynor, B. W.; Filocamo, S. F.; Grinstaff, M. W.; Liu, J. Direct-Writing of Polymer Nanostructures: Poly(thiophene) Nanowires on Semiconducting and Insulating Surfaces. *J. Am. Chem. Soc.* **2002**, *124*, 522–523.
18. Su, M.; Aslam, M.; Fu, L.; Wu, N.; Dravid, V. P. Dip-Pen Nanopatterning of Photosensitive Conducting Polymer Using a Monomer Ink. *Appl. Phys. Lett.* **2004**, *84*, 4200–4202.
19. Lenhert, S.; Sun, P.; Wang, Y. H.; Fuchs, H.; Mirkin, C. A. Massively Parallel Dip-Pen Nanolithography of Heterogeneous Supported Phospholipid Multilayer Patterns. *Small* **2007**, *3*, 71–75.
20. Lee, K. B.; Lim, J. H.; Mirkin, C. A. Protein Nanostructures Formed *via* Direct-Write Dip-Pen Nanolithography. *J. Am. Chem. Soc.* **2003**, *125*, 5588–5589.
21. Lim, J. H.; Ginger, D. S.; Lee, K. B.; Heo, J.; Nam, J. M.; Mirkin, C. A. Direct-Write Dip-Pen Nanolithography of Proteins on Modified Silicon Oxide Surfaces. *Angew. Chem., Int. Ed.* **2003**, *42*, 2309–2312.
22. Zhang, H.; Chung, S. W.; Mirkin, C. A. Fabrication of Sub-50-nm Solid-State Nanostructures on the Basis of Dip-Pen Nanolithography. *Nano Lett.* **2003**, *3*, 43–45.
23. Liu, S. T.; Maoz, R.; Sagiv, J. Planned Nanostructures of Colloidal Gold *via* Self-Assembly on Hierarchically Assembled Organic Bilayer Template Patterns with *in-situ* Generated Terminal Amino Functionality. *Nano Lett.* **2004**, *4*, 845–851.
24. Liu, S. T.; Maoz, R.; Schmid, G.; Sagiv, J. Template Guided Self-Assembly of [Au5(5)] Clusters on Nanolithographically Defined Monolayer Patterns. *Nano Lett.* **2002**, *2*, 1055–1060.
25. Zheng, J.; Zhu, Z.; Chen, H.; Liu, Z. Nanopatterned Assembling of Colloidal Gold Nanoparticles on Silicon. *Langmuir* **2000**, *16*, 4409–4412.
26. Ben Ali, M.; Ondarcuhu, T.; Brust, M.; Joachim, C. Atomic Force Microscope Tip Nanoprinting of Gold Nanoclusters. *Langmuir* **2002**, *18*, 872–876.
27. Garno, J. C.; Yang, Y. Y.; Amro, N. A.; Cruchon-Dupeyrat, S.; Chen, S. W.; Liu, G. Y. Precise Positioning of Nanoparticles on Surfaces Using Scanning Probe Lithography. *Nano Lett.* **2003**, *3*, 389–395.
28. Thomas, P. J.; Kulkarni, G. U.; Rao, C. N. R. Dip-Pen Lithography Using Aqueous Metal Nanocrystal Dispersions. *J. Mater. Chem.* **2004**, *14*, 625–628.
29. Wu, B.; Ho, A.; Moldovan, N.; Espinosa, H. D. Direct Deposition and Assembly of Gold Colloidal Particles Using a Nanofountain Probe. *Langmuir* **2007**, *23*, 9120–9123.
30. Taha, H.; Lewis, A.; Sukenik, C. Controlled Deposition of Gold Nanowires on Semiconducting and Nonconducting Surfaces. *Nano Lett.* **2007**, *7*, 1883–1887.
31. Calleja, M.; Tello, M.; Anguita, J.; Garcia, F.; Garcia, R. Fabrication of Gold Nanowires on Insulating Substrates by Field-Induced Mass Transport. *Appl. Phys. Lett.* **2001**, *79*, 2471–2473.
32. Lee, W. K.; Chen, S. H.; Chilkoti, A.; Zauscher, S. Fabrication of Gold Nanowires by Electric-Field-Induced Scanning Probe Lithography and *in situ* Chemical Development. *Small* **2007**, *3*, 249–254.
33. Li, Y.; Maynor, B. W.; Liu, J. Electrochemical AFM "Dip-Pen" Nanolithography. *J. Am. Chem. Soc.* **2001**, *123*, 2105–2106.
34. Maynor, B. W.; Li, Y.; Liu, J. Au "Ink" for AFM "Dip-Pen" Nanolithography. *Langmuir* **2001**, *17*, 2575–2578.
35. Basnar, B.; Weizmann, Y.; Cheglakov, Z.; Willner, I. Synthesis of Nanowires Using Dip-Pen Nanolithography and Biocatalytic Inks. *Adv. Mater.* **2006**, *18*, 713–718.
36. Rozhok, S.; Piner, R.; Mirkin, C. A. Dip-Pen Nanolithography: What Controls Ink Transport. *J. Phys. Chem. B* **2003**, *107*, 751–757.
37. Weeks, B. L.; Noy, A.; Miller, A. E.; De Yoreo, J. J. Effect of Dissolution Kinetics on Feature Size in Dip-Pen Nanolithography. *Phys. Rev. Lett.* **2002**, *88*, 255505-1–255505-4.
38. Piret, F.; Su, B. L. Effects of pH and Ionic Strength on the Self-Assembly of Silica Colloids to Opaline Photonic Structures. *Chem. Phys. Lett.* **2008**, *457*, 376–380.
39. Einstein, A. On the Motion of Small Particles Suspended in Liquids at Rest Required by the Molecular-Kinetic Theory of Heat. *Ann. Phys. (Leipzig)* **1905**, *17*, 549–560.
40. Nafday, O. A.; Vaughn, M. W.; Weeks, B. L. Evidence of Meniscus Interface Transport in Dip-Pen Nanolithography: An Annular Diffusion Model. *J. Chem. Phys.* **2006**, *125*, 144703-1–144703-4.
41. Hampton, J. R.; Dameron, A. A.; Weiss, P. S. Double-Ink Dip-Pen Nanolithography Studies Elucidate Molecular Transport. *J. Am. Chem. Soc.* **2006**, *128*, 1648–1653.
42. Jang, J. Y.; Schatz, G. C.; Ratner, M. A. Liquid Meniscus Condensation in Dip-Pen Nanolithography. *J. Chem. Phys.* **2002**, *116*, 3875–3886.
43. Jung, H.; Dalal, C. K.; Kuntz, S.; Shah, R.; Collier, C. P. Surfactant Activated Dip-Pen Nanolithography. *Nano Lett.* **2004**, *4*, 2171–2177.
44. Jana, N. R.; Peng, X. G. Single-Phase and Gram-Scale Routes toward Nearly Monodisperse Au and Other Noble Metal Nanocrystals. *J. Am. Chem. Soc.* **2003**, *125*, 14280–14281.
45. Liu, X.; Atwater, M.; Wang, J.; Huo, Q. Extinction Coefficient of Gold Nanoparticles with Different Sizes and Different Capping Ligands. *Colloids Surf., B* **2007**, *58*, 3–7.
46. Woolley, A. T.; Kelly, R. T. Deposition and Characterization of Extended Single-Stranded DNA Molecules on Surfaces. *Nano Lett.* **2001**, *1*, 345–348.